JACS
JOURNAL OF THE AMERICAN CHEMICAL SOCIETY

ARTICLE

pubs.acs.org/JACS

Interleaflet Interaction and Asymmetry in Phase Separated Lipid Bilayers: Molecular Dynamics Simulations

Jason D. Perlmutter and Jonathan N. Sachs*

Biomedical Engineering, University of Minnesota, Minneapolis, Minnesota 55455, United States

Supporting Information

ABSTRACT: In order to investigate experimentally inaccessible, molecular-level detail regarding interleaflet interaction in membranes, we have run an extensive series of coarse-grained molecular dynamics simulations of phase separated lipid bilayers. The simulations are motivated by differences in lipid and cholesterol composition in the inner and outer leaflets of biological membranes. Over the past several years, this phenomenon has inspired a series of experiments in model membrane systems which have explored the effects of lipid compositional asymmetry in the two leaflets. The simulations are directed at understanding one potential consequence of compositional asymmetry, that being regions of bilayers where liquid-ordered (L_o) domains in one leaflet are opposite liquid-disordered (L_d) domains in the other leaflet (phase asymmetry). The simulated bilayers are of two sorts: 1) Compositionally symmetric leaflets where each of the two leaflets contains an identical, phase separated (L_o/L_d) mixture of cholesterol, saturated and unsaturated phospholipid; and 2) Compositionally asymmetric leaflets, where one leaflet contains a phase separated (L_o/L_d) mixture while the other contains only unsaturated lipid, which on its own would be in the L_d phase. In addition, we have run simulations where the lengths of the saturated lipid chains as well as the mole ratios of the three lipid components are varied. Collectively, we report on three types of interleaflet coupling within a bilayer. First, we show the effects of compositional asymmetry on acyl chain tilt and order, lipid rotational dynamics, and lateral diffusion in regions of leaflets that are opposite L_o domains. Second, we show substantial effects of compositional asymmetry on local bilayer curvature, with the conclusion that phase separated leaflets resist curvature, while inducing large degrees of curvature in an opposing L_d leaflet. Finally, in compositionally symmetric, phase separated bilayers, we find phase asymmetry (domain antiregistration) between the two leaflets occurs as a consequence of mismatched acyl chain-lengths in the saturated and unsaturated lipids.

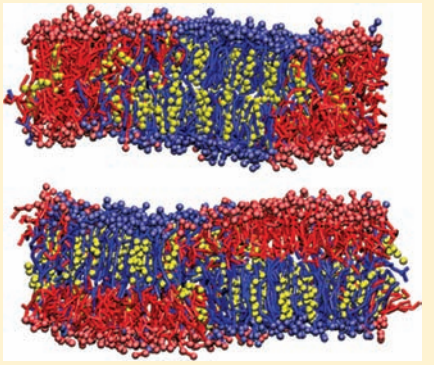

INTRODUCTION

Biological membranes are far from homogeneous, and the list of ways in which they differ from the canonical fluid mosaic model[1] is ever expanding.[2] Of these, two appear to have particular significance in dictating how cells organize their membrane bound protein machinery. First, phase separation in the plane of the bilayer is now thought to be an important functional feature of biological membranes.[3−7] Biophysical experiments and computational studies of synthetic model systems (e.g., lipid vesicles) have shown unambiguously that cholesterol preferentially associates with saturated lipids and that this induces a phase separation of liquid-ordered (L_o) and disordered (L_d) domains.[8−14]

A less-well understood aspect of biological membranes is the consequence of different lipid and cholesterol compositions in the two leaflets.[11,15−20] For example, in mammalian plasma membranes the majority of sphingomyelin is found in the outer leaflet.[21] Since sphingomyelin is thought to be the primary component of lipid rafts,[22] its asymmetric distribution has raised a set of important questions: how does the compositional asymmetry affect the phase behavior of the inner leaflet? That is, if the outer leaflets of biological membranes contain L_o domains, while the inner leaflet composition is such that in isolation it should be uniformly disordered,[12,23] then what thermodynamic characteristics does that inner leaflet actually possess? How are the two leaflets coupled? Does *compositional* asymmetry lead to *phase* asymmetry (i.e., L_o and L_d domains directly opposite one another in the two leaflets), or conversely, are domains induced in the inner leaflet resulting in phase symmetry?

That biological membranes are compositionally asymmetric has been repeatedly verified.[11,15−20] However, experiments on domains in biological membranes rely upon methods such as detergent extraction that are unable to resolve the phases of the individual leaflets. Therefore, validating the existence of phase asymmetry in biological membranes remains very difficult, making critical the insights available from experiments on model, synthetic lipid bilayers. Among the first such experiments that addressed this question—if and how one leaflet affects the structure and thermodynamic phase behavior of an apposed leaflet—used asymmetric ion distributions to investigate how the

Received: August 3, 2010
Published: April 07, 2011

two leaflets of a bilayer are coupled. The results were ambiguous: in some cases an interleaflet structural perturbation could be observed by an altered phase transition temperature;[24,25] in other cases no effect was observed.[26]

More recently, fluorescence microscopy experiments using synthetic lipid bilayers with an asymmetric lipid composition, along with dyes that favor either the L_o or L_d phases, have yielded significant insight, though again no clearly consistent picture has emerged. Some experiments have suggested that an L_o domain in one leaflet can induce an L_o domain in an opposing leaflet that would, on its own, be L_d.[21,27−30] Thus, while these bilayers are compositionally asymmetric, they were suggested to be phase symmetric. For example, one experiment studied the effect of an L_o/L_d phase separated leaflet composed of a 2:2:1 mixture of DOPC:DPPC:Cholesterol on an opposing leaflet composed of a mixture of solely unsaturated lipids (DOPC, DOPE, and DOPS).[29] Visual inspection of the partitioning of one L_o-favoring dye and another L_d-favoring dye led to the conclusion that an L_o domain had been induced in the leaflet composed solely of unsaturated lipids. On the other hand, alteration of phase-state across leaflets of asymmetric bilayers appears to be highly sensitive to the lipid constituents. A separate experiment on a compositionally asymmetric bilayer containing a domain forming mixture of brain PC, brain SM, and cholesterol in one leaflet failed to alter dye partitioning in an opposing leaflet composed of DOPC, meaning that this particular compositionally asymmetric bilayer remained phase asymmetric.[29]

While striking qualitative results, these findings left open the possibility that intermediate levels of L_o-favoring dye partitioning indicate the existence of an intermediate phase in the regions opposite an L_o domain. This possibility was further elaborated in the experiments of Collins et al.[27] Again using dye partitioning experiments in compositionally asymmetric bilayers, three levels of intensity were observed. Using an elegant free-energy model, the study identified three corresponding configurations of bilayer-spanning phases across the two leaflets: L_o/L_o, L_d/L_d, and L_o/L_d. The latter, identified in the experiments as regions with an intermediate intensity between L_o and L_d, was termed a bilayer-spanning 'mixed' phase, where the lipid components are likely more ordered than L_d but less ordered than L_o.[27]

One important clarification regarding these experiments on asymmetric bilayers that has direct bearing on the simulation strategy employed here is that they were all performed under nonequilibrium conditions. Specifically, all measurements were made immediately after formation of the asymmetric bilayers, ensuring that over the time-scale of the experiments there is no phospholipid flip-flop between the leaflets.[27−30] That is, as Collins et al.[27] pointed out, in experiments under these conditions the lipid chemical potentials are not necessarily equal in the two leaflets. Performing the experiments in this way most closely models the thermodynamic state of biological membranes, where the lipid asymmetry is established by enzymes called flippases, which utilize ATP in maintaining the nonequilibrium, asymmetric distributions of lipids.[31]

A second important issue regarding phase asymmetry is the observation that in compositionally symmetric bilayers there is a tendency for L_o domains in opposing leaflets to overlay, or register (that is, to be phase symmetric),[30,32−34] though again a number of exceptions have been observed.[35−37] Similar inconsistencies have been observed in the case of solid domains, which showed registration for one lipid mixture, but not for another.[38] Theoretical treatments have explored the energetic underpinnings of domain registration (phase symmetry) vs antiregistration (phase asymmetry), suggesting that a fine balance between an interleaflet line tension at the bilayer midplane and an intraleaflet tension at the interface of domains within each leaflet plays a central role.[39−43] Nevertheless, despite the technically elegant accomplishments of recent experiments and theoretical treatments, it currently remains undetermined exactly how leaflets of a bilayer are coupled together, why certain mixtures induce domain formation across the bilayer and others do not, and whether biological membranes are phase symmetric or asymmetric.[39,44]

In order to examine the interactions between leaflets in bilayers with at least one phase separated leaflet, we make use of computational molecular dynamics (MD) simulations. Previously, all-atom MD simulations have been used to study the structure of single phase lipid bilayers with a compositional asymmetry of lipids and ions, for example observing the effects on the bilayer electrostatic potential.[45−54] However, domain formation requires time- and length-scales inaccessible to all-atom simulations. To address this, coarse-grained MD (CGMD) force fields have been developed. In CGMD, atoms are grouped together into multiatomic units, reducing the computational cost and allowing investigation of longer time- and length-scales. In particular, using the Martini CGMD force field,[55] bilayers with compositional asymmetry were found to be stable over a multiμs simulation[56] and *de novo*, registered L_o domain formation in a compositionally symmetric bilayer has been observed.[14] Additionally, CGMD simulations have studied possible interleaflet effects due to antiregistered (phase asymmetric) solid domains[57] and solid supported lipid bilayers.[58] The success of these simulations suggests that this type of computational modeling is a potent strategy for understanding the effects of compositional asymmetry on bilayer structure and phase behavior.

In this study, we have used CGMD to model phase separated, compositionally symmetric and asymmetric lipid bilayers. The asymmetric bilayers are initiated with a single-component, single phase (L_d) top leaflet opposing a three-component, laterally phase separated (L_o/L_d) bottom leaflet. Over the course of the simulations, we find an increase in the degree of lipid order in the region of the top leaflet that is opposite an L_o domain, as quantified through lipid chain tilt angle and average lipid chain order parameter. We have also found a decrease in order in the region of the single-component, top leaflet opposite an L_d domain. Further, we report a novel finding regarding the induction of local curvature in the single-component leaflet of the asymmetric bilayers that may be correlated with this change in order.

We have also found an intriguing connection between lipid chain-length and phase symmetry in compositionally symmetric bilayers. Early models of isolated L_o and L_d domains that were based upon NMR measurements suggested the importance of the relative lengths of acyl chains and cholesterol in dictating the midplane organization of the molecular constituents, with a focus on the ability of the molecules to interlock.[59,60] Inspired by this paradigm, we have run a series of simulations in which we have varied the length of the saturated lipid in only the L_o domains and show that in compositionally symmetric bilayers L_o domains containing lipids with shorter chains are in register (phase symmetric), whereas those containing lipids with longer-chains are antiregistered (phase asymmetric). By varying the mole ratios

of the constituent lipids, we have further explored the extent of this registration phenomenon and suggest a fine balance between bilayer curvature stress and domain mixing. These findings highlight how a height-mismatch between the L_o and L_d domains within a leaflet can impact interleaflet organization. Collectively, our findings expand upon the current understanding of how compositional asymmetry is coupled to the phase behavior and structure of individual leaflets, offering a revised and higher-resolution picture of the biophysics of interleaflet coupling.

METHODS

System Construction. Bilayer systems were built using the Martini CGMD force field,[55] which uses an approximate mapping of 4 non-hydrogen atoms per bead. In addition to cholesterol, we have used four different lipids: CG di-4:0 roughly corresponds to the all-atom structure of di-16:0; di-5:0 corresponds to di-20:0; di-6:0 corresponds to di-24:0; and di-4:2 corresponds to di-18:2. First, we simulated three compositionally symmetric, ternary bilayers, all of which phase separated over the course of the simulations. These 2:2:1 systems consisted of 256 unsaturated lipids (di-4:2PC), 256 saturated (either di-4:0PC, di-5:0PC, or di-6:0PC) lipids, 128 cholesterols, and ~10,000 water beads. The bilayer containing di-4:2PC, di-4:0PC, and cholesterol is identical to the one we used previously to model L_d/L_o domain formation.[61] An initial starting configuration for each of the symmetric systems was obtained through a 400 ns simulation of a 2:2:1 mixture of di-4:2PC, di-4:0PC, and cholesterol, at an increased temperature (400 K) which randomized the lateral distribution of lipids in order to avoid starting configuration bias. Symmetric bilayers containing longer-chain lipids as the saturated lipid component used the same starting configuration, with the only modification being the addition of either 1 (di-5:0PC) or 2 (di-6:0PC) acyl chain groups (type C1) onto the *sn*-1 and *sn*-2 chains of the di-4:0PC. Symmetric bilayers containing a different molar ratio, either 1:2:1 or 4:2:1, were built such that they maintain as closely as possible the same number of total lipids as in the other symmetric bilayers. As described below, based on visualization and quantitative analysis we conclude that each saturated lipid forms the L_o phase with cholesterol, rather than the gel phase.[62]

In order to build asymmetric bilayers, it was necessary to ensure that each leaflet of the bilayer would have the same lateral area. Pairing together leaflets with different areas could lead to a compression or expansion, an artifact which would alter the structure of the bilayer[54,63,64] and possibly cause buckling. That we were successful in avoiding this artifact is detailed below. Thus, in order to assemble a bilayer containing a ternary, laterally separated leaflet opposite a single-phase, single-component leaflet we first needed to perform a series of compositionally symmetric simulations. This was done so as to determine the appropriate number of lipids to include in each leaflet of the asymmetric bilayers. Then, using the areas determined from these equilibrated symmetric bilayer simulations, we built asymmetric bilayers that consist of one ternary leaflet and one single-component (di-4:2PC), single-phase leaflet. In order to determine the sizes (i.e., number of lipids) of the di-4:2PC leaflets needed to match the equilibrated areas of the ternary leaflets, a series of relatively brief (500 ns) simulations of single-component, di-4:2PC bilayers were run in order to test how the area depends upon system size (Figure S1). This series of simulations resulted in an average area per di-4:2PC of 0.742 nm^2. Based on this analysis, a leaflet composed of 237 di-4:2PC lipids matched the area of the compositionally symmetric bilayers containing di-4:0 PC; 233 di-4:2PC lipids matched the compositionally symmetric bilayer containing di-5:0PC; and 232 di-4:2PC lipids matched the compositionally symmetric bilayer containing di-6:0. An initial configuration was built for each asymmetric bilayer by joining the corresponding top leaflet of the single component, di-4:2PC bilayer with the bottom leaflet of the symmetric, ternary bilayer (using its starting configuration, which was not yet phase separated), and then solvating in a water box of ~10,000 water beads. A symmetric, single-component bilayer containing two leaflets each composed of 237 di-4:2PC lipids was also simulated. Additional systems were built, in which 10, 20, or 30 cholesterol molecules were added to this bilayer, in order to provide a control that was necessary for handling the analysis of systems in which cholesterols were found to flip-flop between leaflets. The set of simulated bilayers along with their leaflet lipid and cholesterol distributions are summarized in Table 1.

Table 1. Lipid and Cholesterol Composition of the Top and Bottom Leaflets in Each Simulation

Top Leaflet	Bottom Leaflet
Symmetric Simulations	
di-4:2, di-4:0, Chol (128:128:64)	di-4:2, di-4:0, Chol (128:128:64)
di-4:2, di-5:0, Chol (128:128:64)	di-4:2, di-5:0, Chol (128:128:64)
di-4:2, di-6:0, Chol (128:128:64)	di-4:2, di-6:0, Chol (128:128:64)
Symmetric Simulations (Altered Ratios)	
di-4:2, di-5:0, Chol (80:160:80)	di-4:2, di-5:0, Chol (80:160:80)
di-4:2, di-5:0, Chol (184:92:36)	di-4:2, di-5:0, Chol (184:92:36)
Asymmetric Simulations	
di-4:2 (237)	di-4:2, di-4:0, Chol (128:128:64)
di-4:2 (233)	di-4:2, di-5:0, Chol (128:128:64)
di-4:2 (232)	di-4:2, di-6:0, Chol (128:128:64)
Control Simulations	
di-4:2 (237)	di-4:2 (237)
di-4:2 + 5 Chol (237:5)	di-4:2 + 5 Chol (237:5)
di-4:2 + 10 Chol (237:10)	di-4:2 + 10 Chol (237:10)
di-4:2 + 15 Chol (237:15)	di-4:2 + 15 Chol(237:15)
di-4:2, di-4:0 (128:128)	di-4:2, di-4:0, Chol (128:128:64)
di-4:2 (227)	di-4:2, di-4:0, Chol (128:128:64)

It is important to clarify that the lipid distribution in the simulated bilayers is intentionally in a nonequilibrium state. Though equilibration is typically an important criterion for convergence of particle-based molecular simulations, in this case the simulations are modeling a set of nonequilibrium experiments where lipid redistribution between the leaflets is not the appropriate convergence criterion. More specifically, in biological membranes compositional asymmetry is maintained by enzymes which frequently require energetic input in the form of ATP.[31] In the absence of this enzymatic machinery, numerous experiments which have constructed model bilayers with compositional asymmetry have been careful to avoid phospholipid flip-flop, which leads to a loss of the asymmetry on a time-scale of hours to days.[27−30,36,65,66] Therefore, in order to study the biologically relevant asymmetry in a simple biophysical model, experiments have been performed before the phospholipids have a chance to flip and equilibrate.[27−30,36,65,66] Cholesterol, which flips much more quickly, does redistribute in the experimental time frame. Our simulations therefore follow the strategy used in these experiments: we artificially create a compositionally asymmetric bilayer and describe its structure after equilibration of all structural features except for redistribution of phospholipids between the leaflets (therefore occupying a local, but not global, free energy minimum). Ensuring convergence of these properties, which include alterations in local curvature, was critically important and is described below. It is therefore appropriate that, on the time-scale of the simulations, no instances of phospholipid flip-flop are observed, and each leaflet's phospholipid composition does not change from the starting configuration through the duration of each simulation. Also appropriate to the experiments we are modeling, cholesterol redistribution between the leaflets is observed,

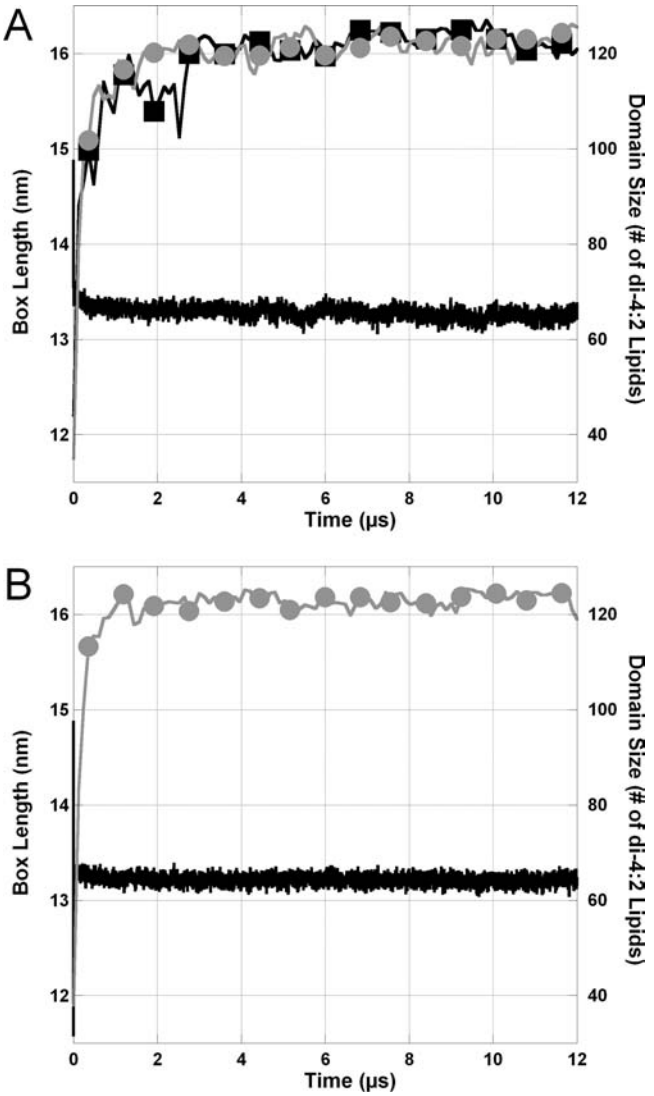

Figure 1. Representative timeseries showing equilibration of the simulations on the μs time scale. (A) [di-4:2, di-4:0, Chol]/[di-4:2, di-4:0, Chol]. (B) [di-4:2]/[di-4:2, di-4:0, Chol]. Box length (black line) and size of the disordered domain (top leaflet = black squares; bottom leaflet = gray circles). Corresponding data for the other simulations are available as Figure S2.

and convergence of that aspect is carefully monitored and controlled for as described above and explained below. Given that our simulations were not intended to converge to the global equilibrium state, it was critical to run multiple starting configurations in order to ensure that our reported findings are statistically reliable. To this end, we have in most instances run three distinct initial configurations. In each case, these separate simulations yielded indistinguishable results, increasing confidence in the robustness of our findings. Where convenient we present the standard error, treating the averages from the three simulations as independent samples. Otherwise, the results presented are from the initial, random configuration simulations, described above. Additional details regarding construction of these different initial configurations are available as Supporting Information.

Simulation Details. Simulations were run with Gromacs version 3.3.3 and 4.0.7,[67] using periodic boundary conditions and a constant number of particles (N), pressure (P), and temperature (T). The Berendsen pressure coupling scheme was applied in a semi-isotropic manner resulting in a tensionless bilayer, where the *xy*-axes define the lateral plane of the bilayer and the *z*-axis is normal to the global bilayer surface. We utilize the convention of describing the effective time sampled as a 4-fold increase over the simulation time, due to a "smoothing" of the energy profile in coarse grain simulation.[55] Simulations were run with a time step of 30 fs for a duration of 12 μs effective time, at a temperature of 295 K.[14] The results presented here total more than 350 μs of simulation.

Analysis Details. Analysis of these simulations was performed using Gromacs,[67] VMD,[68] and a set of in-house Perl scripts. Based on equilibration of the lateral structure (Figure 1), all analysis was performed on time points starting after 2.4 μs, unless otherwise noted.

Analysis of per-leaflet density distributions required nontrivial assignment of cholesterol molecules. Cholesterol has been shown to flip-flop rapidly between leaflets as well as to stably occupy intermediate states at the bilayer midplane, and thus in these instances ascribing a cholesterol to one of the leaflets can be somewhat ambiguous.[69,70] For each cholesterol, we identified the closest lipid in the *xy*-plane in both leaflets (based on the position of the first bead in the acyl chain) and then used the minimum of the two distances in *z* between the cholesterol hydroxyl group and those lipids to assign it to a leaflet. In order to preserve the information on the relative density of cholesterol in the two leaflets, the density of cholesterol is normalized for the bilayer, while the lipid density is normalized per leaflet.

To analyze the degree of lipid order, we utilize the lipid chain segmental order parameter

$$P_2 = \frac{1}{2}(3\cos^2\langle\theta\rangle - 1) \quad (1)$$

where θ is the angle formed by the bond segment and the global bilayer normal (z) axis. Data presented are the average of each bond segment, as in ref 14.

A parameter we have used for analyzing the dynamics is the lipid rotational autocorrelation function, defined as

$$C(\tau) = \frac{\langle \vec{C}_i(t)\cdot\vec{C}_i(t+\tau)\rangle}{\langle \vec{C}_i(t)\cdot\vec{C}_i(t)\rangle} \quad (2)$$

where $\vec{C}$ is the vector connecting the lipid backbone groups, τ is the lag time, and the brackets indicate an average over time (t) and lipids (i). The resulting function was approximated as an exponential decay

$$C(\tau) \approx e^{(-\tau/\chi)} \quad (3)$$

where χ is the characteristic decay time. Fitting using a larger number of terms, such as through a double[71] or triple[72] exponential function yields more accurate fitting. However, using eq 3 provided reasonable agreement ($R^2 > 0.94$) and allowed us to succinctly communicate the change in structure induced by interleaflet communication.

A second parameter we have used to analyze the bilayer dynamics is the lateral diffusion coefficient, defined as

$$\langle r^2\rangle = 4Dt \quad (4)$$

where $\langle r^2\rangle$ is the 2-dimensional mean squared displacement (corrected for the leaflet center of mass motion), D is the diffusivity, and t is time. The MSD is linear in the long time limit, and thus the slope of the MSD plotted against time was used to determine D.

RESULTS

Compositional Asymmetry. In this section we present results on how lipid compositional asymmetry affects the structure and dynamics of bilayers containing a single-component leaflet opposite a three-component, phase separated leaflet. As controls, we have run compositionally symmetric bilayers as well. As

described in detail in the Methods section, the top leaflet of each of the simulated, compositionally asymmetric bilayers is composed of di-4:2PC, a coarse-grained model of di-18:2PC which on its own (in a compositionally symmetric, single-component di-4:2PC bilayer) is in the L_d phase at the simulated temperature.[14] The bottom leaflets of the compositionally asymmetric bilayers are composed of a ternary mixture of di-4:2PC, cholesterol, and a saturated lipid: either di-4:0PC (a CG representation of di-16:0PC), di-5:0PC (representing di-20:0PC), or di-6:0PC (representing di-24:0PC). The di-4:2PC, di-4:0PC, and cholesterol mixture has been shown to phase separate in previous simulations of compositionally symmetric bilayers, with the di-4:2 lipids segregating into an L_d phase region, and the saturated lipid and cholesterol collectively forming an L_o phase region.[14,61] Throughout the text, bilayers are identified by citing the lipid content of the top and bottom leaflets as [top]/[bottom]. For example, [di-4:2]/[di-4:2, di-4:0, Chol] indicates a single-component leaflet on top, and a ternary, phase separated leaflet on the bottom. Table 1 provides a summary of the simulated bilayers.

In order to ensure convergence of domain structures within each leaflet, we have quantified both the bilayer lateral area and the domain size. As a representative example, Figure 1 presents results from the symmetric [di-4:2, di-4:0, Chol]/[di-4:2, di-4:0, Chol] and the asymmetric [di-4:2]/[di-4:2, di-4:0, Chol] bilayers, showing nearly complete L_o/L_d phase separation in the leaflets containing ternary mixtures within the first 2 μs of the simulations.[14,61] The rate and extent of domain formation was quantified by the largest number of diunsaturated lipids in contact with each other (defined by a 1.2 nm cutoff between phosphate groups[61]). Figure 1 also shows the equilibration of the bilayer lateral area (*xy*-dimensions), a parameter that needed to be carefully monitored in the case of the asymmetric bilayers (as described in Methods). In the symmetric, single phase bilayers ([di-4:2]/[di-4:2], and in the control simulations containing cholesterol, Figure S2) the lateral areas equilibrate within the first 10 ns of the simulations. Slower area convergence in the ternary mixtures ($\sim$2 μs) is due to the colocalization of cholesterol with the saturated lipid and resultant area condensation.[52,73−76] The equilibration of domains and bilayer areas in the simulations containing longer-chain lipids is similar and is presented in Figure S2. We conclude that the time-scale of our simulations is sufficient to observe converged behavior, and we have utilized time-points after 2.4 μs for all analysis. Other properties that we discuss below (lipid tilt, diffusion, and local curvature) are also converged on this time-scale (Figure S3).

Figure 2 shows the core results for our questions regarding compositional asymmetry. In this initial analysis, we restrict our attention to the simulations with di-4:0 saturated lipid, reserving analysis of the longer-chain lipids for the next section. The first 3 columns of Figure 2 show the densities of the various lipid components (di-4:2, di-4:0, and cholesterol) in the plane of each leaflet. As expected, in the compositionally symmetric control [di-4:2]/[di-4:2] bilayer, the lipid is evenly distributed throughout each leaflet. In each of the ternary leaflets, including both leaflets of the symmetric [di-4:2, di-4:0, Chol]/[di-4:2, di-4:0, Chol] bilayer and the bottom leaflet of the asymmetric [di-4:2]/[di-4:2, di-4:0, Chol] bilayer, the di-4:2 phase separates from the di-4:0 and cholesterol, as was previously indicated in Figure 1. In the symmetric bilayer, the L_o domains (consisting of di-4:0 and cholesterol) in the two leaflets overlay, indicating that they are in register (phase symmetric), as has been previously reported for a similar system.[14]

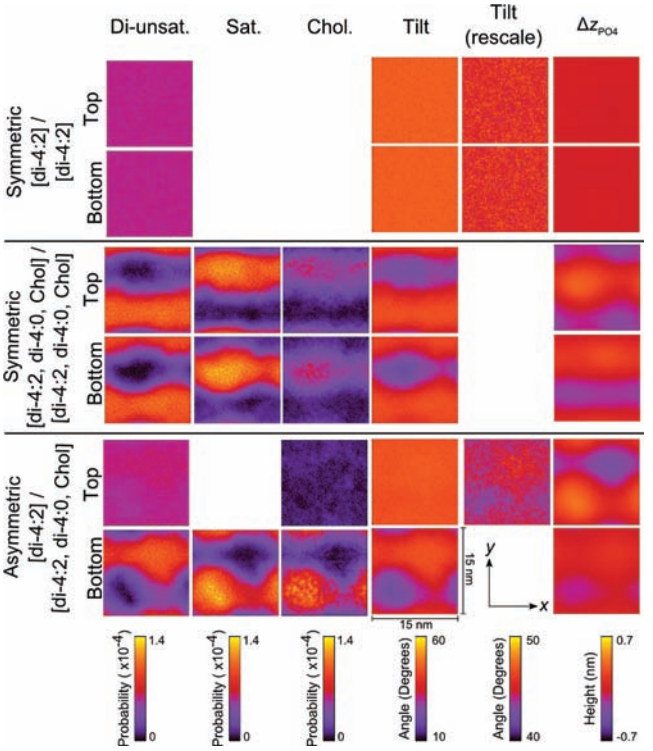

Figure 2. The effect of phase asymmetry on per-leaflet component distributions (diunsaturated, saturated, and cholesterol), lipid tilt, and surface curvature (Δz_{PO4}) for the [di-4:2]/[di-4:2], [di-4:2, di-4:0, Chol]/[di-4:2, di-4:0, Chol], and [di-4:2]/[di-4:2, di-4:0, Chol] bilayers. Periodic images have been included so that each panel is 15 × 15 nm.

The third column of Figure 2 demonstrates the lateral localization of cholesterol into regions that overlap neatly with the di-4:0 distributions. Because cholesterol is known to flip-flop rapidly between leaflets on the time-scale of the experiments we are modeling,[69,70] its equilibrium distribution should be independent of the starting configuration. As expected, in the symmetric bilayer cholesterol distributes evenly between the two leaflets as indicated by the same intensity in the cholesterol panels. However, in the asymmetric bilayer $\sim$15% of the cholesterol redistributes to the top (di-4:2) leaflet. The cholesterol distributions converged within the first 200 ns of each simulation, remaining approximately unchanged throughout the remainder of the simulations (Figure S4), despite the fact that individual cholesterol molecules continued to flip-flop between the leaflets throughout. The small amount of cholesterol that ends up in the top (di-4:2) leaflet of the asymmetric bilayer ($\sim$10 cholesterol molecules) may itself have an internal effect on that leaflet's structure that is independent of the effect of compositional asymmetry. In order to address any potential effects of this, we have run a series of control simulations containing symmetric distributions of di-4:2 and increasing amounts of cholesterol. The lateral densities from these simulations are presented in Figure S5.

The fourth and fifth columns of Figure 2, along with Figure S6, begin to address the question of whether the L_o domains in the bottom leaflet of the compositionally asymmetric simulations alter the properties, or even induce a phase transition, in the single-component, top leaflet. Assigning a phase based upon the dynamic and structural properties of lipids in a simulated bilayer

Table 2. Lipid Tilt, Rotational Autocorrelation, and Lateral Diffusion

bilayer	mean tilt (°)	approximate rotation decay time (ns)	diffusion coefficient (10^{-7} cm^2/s)
di-4:2 Lipids from the Top Leaflet			
Single Component [di-4:2]/[di-4:2]	45.8 ± 0.01	4.22 ± 0.003	2.07 ± 0.02
Symmetric [di-4:2, di-4:0, Chol]/[di-4:2, di-4:0, Chol]	43.8 ± 0.13	6.50 ± 0.02	0.74 ± 0.01
Symmetric [di-4:2, di-5:0, Chol]/[di-4:2, di-5:0, Chol]	43.3 ± 0.43	6.63 ± 0.12	0.79 ± 0.06
Symmetric [di-4:2, di-6:0, Chol]/[di-4:2, di-6:0, Chol]	42.4 ± 0.06	6.42 ± 0.11	0.68 ± 0.03
Asymmetric [di-4:2]/[di-4:2, di-4:0, Chol]	44.4 ± 0.05	4.71 ± 0.01	1.94 ± 0.05
Asymmetric [di-4:2]/[di-4:2, di-5:0, Chol]	44.9 ± 0.03	4.62 ± 0.01	1.84 ± 0.11
Asymmetric [di-4:2]/[di-4:2, di-6:0, Chol]	45.0 ± 0.05	4.66 ± 0.02	1.89 ± 0.07
di-4:0 Lipids from the Top Leaflet			
Symmetric [di-4:2, di-4:0, Chol]/[di-4:2, di-4:0, Chol]	22.6 ± 0.24	35.80 ± 1.80	0.39 ± 0.05
di-5:0 Lipids from the Top Leaflet			
Symmetric [di-4:2, di-5:0, Chol]/[di-4:2, di-5:0, Chol]	25.2 ± 0.30	54.79 ± 2.41	0.32 ± 0.01
di-6:0 Lipids from the Top Leaflet			
Symmetric [di-4:2, di-6:0, Chol]/[di-4:2, di-6:0, Chol]	25.1 ± 0.19	78.13 ± 2.00	0.18 ± 0.01

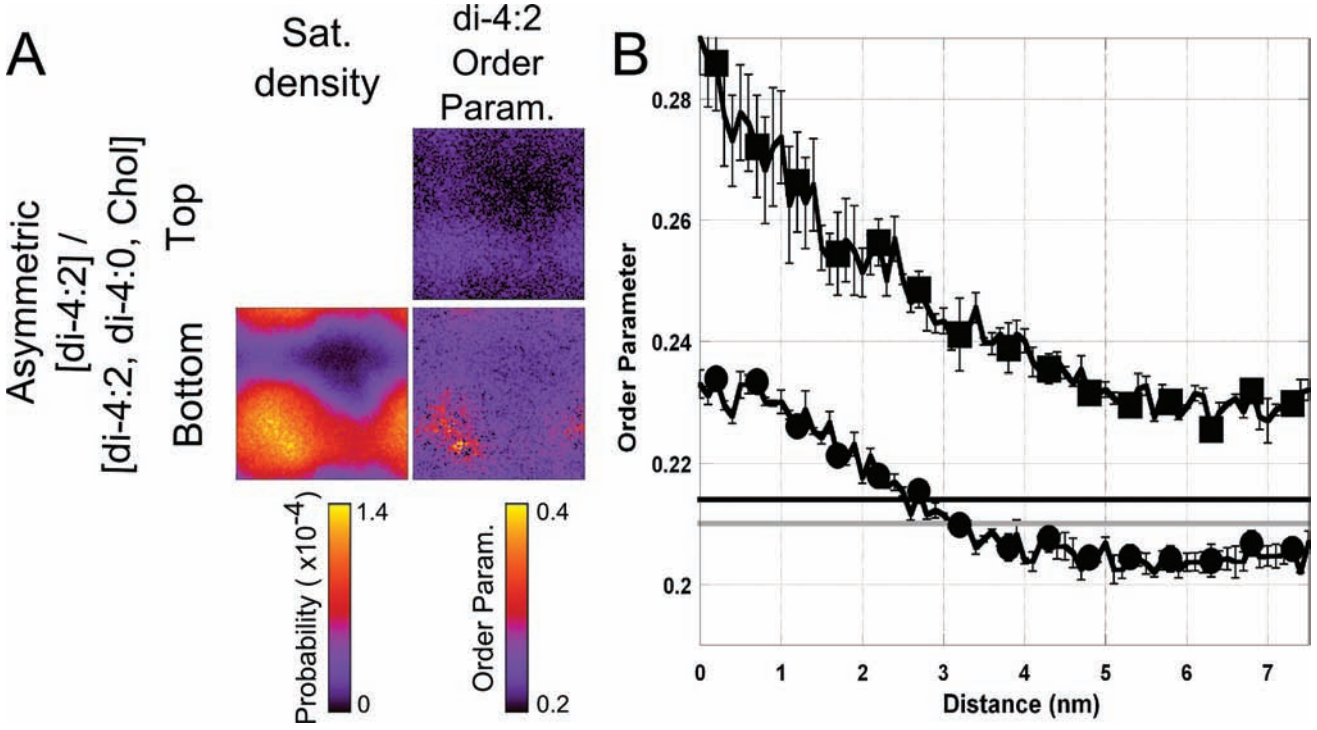

Figure 3. The segmental order parameter of di-4:2 in the [di-4:2]/[di-4:2, di-4:0, Chol] bilayer in the *xy* plane (A) and averaged in 1-dimension with the L_o domain center at $x = 0$ (B). The asymmetric bilayer shows an intraleaflet effect in the bottom leaflet (squares) and an interleaflet effect in the top leaflet (circles). Di-4:2 single component (gray) and +20 cholesterols (black) are provided for comparison.

is nontrivial. Our efforts to do so for the top leaflet of the asymmetric bilayers are based upon di-4:2 lipid tilt and the corresponding average lipid chain order parameter, rotational autocorrelation and diffusion, each of which is quantitatively different in the L_o and L_d phases (Table 2). We define lipid tilt by the angle made by the vector connecting the first and last beads of the lipid chain and the global bilayer normal. As reported in Table 2, in the [di-4:2]/[di-4:2] bilayer the average lipid tilt is 45.8 ± 0.01°. In the symmetric phase separated bilayer ([di-4:2, di-4:0, Chol]/[di-4:2, di-4:0, Chol]), the bilayer averaged di-4:2 lipid tilt is reduced by 2.0°. This *intra*-leaflet effect has been previously attributed to the fact that as unsaturated lipids enter, or neighbor, an ordered domain they adopt a more ordered state.[14,77]

The effect of compositional asymmetry on di-4:2 lipid tilt in the entirety of the top leaflet of the [di-4:2]/[di-4:2, di-4:0, Chol] bilayer—an *inter*-leaflet effect—is only slightly less than the *intra*-leaflet effect, where the average di-4:2 lipid tilt is reduced by 1.4° relative to the [di-4:2]/[di-4:2] bilayer. However, the experimental findings suggest that the focus should be on the region directly opposing the L_o domain. In the fifth column of

dx.doi.org/10.1021/ja106626r |*J. Am. Chem. Soc.* 2011, 133, 6563–6577

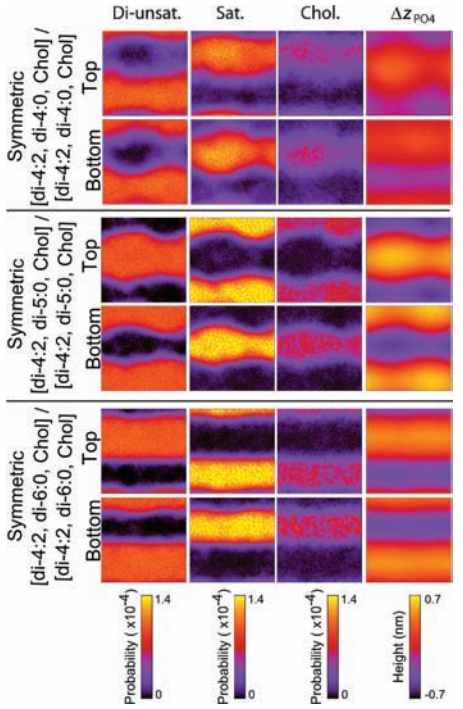

Figure 4. The effect of height mismatch on per-leaflet component distributions (diunsaturated, saturated, and cholesterol) and surface curvature for the [di-4:2, di-4:0, Chol]/[di-4:2, di-4:0, Chol], [di-4:2, di-5:0, Chol]/[di-4:2, di-5:0, Chol], and [di-4:2, di-6:0, Chol]/[di-4:2, di-6:0, Chol] bilayers.

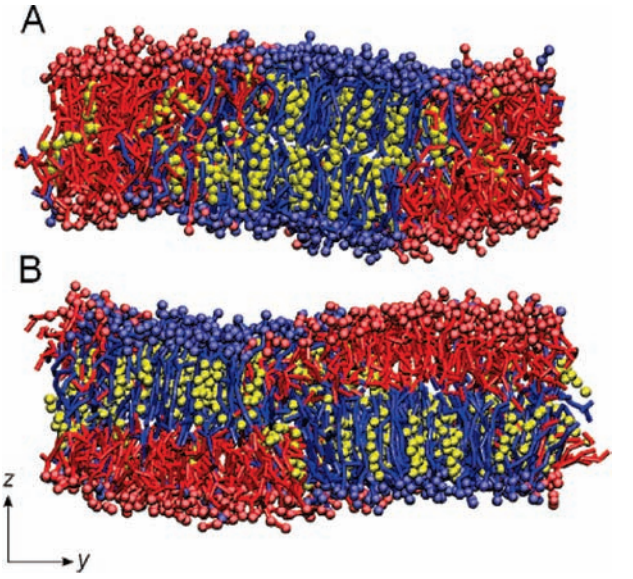

Figure 5. — Snapshots illustrating (A) domain registration in the [di-4:2, di-4:0, Chol]/[di-4:2, di-4:0, Chol] bilayer and (B) antiregistration in the [di-4:2, di-5:0, Chol]/[di-4:2, di-5:0, Chol] (2:2:1) bilayer. Color Scheme: Saturated lipids — blue, diunsaturated lipids — red, cholesterol — yellow. Water has been removed for clarity.

Figure 2, we have readjusted the color scale in order to highlight the effect of tilt in that region alone, where the calculated tilt angles are reduced by as much as 2.2° in the region directly opposite the L_o domain, relative to the [di-4:2]/[di-4:2] bilayer. Based on the set of cholesterol control simulations, we are able to attribute this reduction in tilt primarily to the effect of phase asymmetry, as the presence of small amounts cholesterol in that leaflet itself causes a reduction in tilt of <1° (see Figure S5).

Figure 3 further describes the interleaflet ordering effect as quantified through the lipid chain order parameter, which has been used previously to describe the behavior of saturated and unsaturated lipids in both L_o and L_d domains.[14] This order parameter, shown in two-dimensions in Figure 3A, describes the alignment of each bond vector with the bilayer normal axis, with larger values indicating a more aligned, and more ordered state (eq 1). In simulations of a related, compositionally symmetric ternary mixture, the di-4:2 order parameter was found to increase by ∼30% when the lipid is in the L_o domain rather than its more probable location (i.e., in the L_d domain).[14] Likewise, the di-4:0 order parameter was found to decrease by ∼25% when in the L_d domain. From our simulations, we consider the value of 0.21 obtained from the single component [di-4:2]/[di-4:2] bilayer as a baseline for evaluating the magnitude of changes in ordering. Within the L_o domain of the bottom leaflet of the [di-4:2]/[di-4:2, di-4:0, Chol] bilayer, the di-4:2 order parameter increases in magnitude by as much as ∼38% (to 0.29). In the opposite leaflet, in particular directly across from the center of the L_o domain, the interleaflet effect increases the di-4:2 order by as much as ∼10% (to 0.23). The magnitude of this interleaflet effect is non-negligible, though perhaps less than expected if that region of the leaflet had been induced to have full L_o-character. As evident in Figure 3B, the magnitude of the interleaflet ordering effects are greatest at the domain centers, though there are still substantial effects observed at the domain peripheries. The effect extends out radially by ∼3 nm from the center of the region directly opposite the L_o domain, corresponding to an area of ∼30 nm^2 (or that of ∼40 lipids (Figure S1)). Thus the interleaflet effect is felt in a region of the top leaflet of ∼30% the total extent of the domain. There is also a weaker disordering effect in the region of the top leaflet that is opposite the L_d domain in the bottom, ternary leaflet, which will be described in more detail below. Also included in the figure is the di-4:2 order parameter from the cholesterol control simulation which, as with tilt, confirms that the interleaflet effect on lipid order is not due solely to the presence of the small number of cholesterols which flipped into the leaflet. We have also calculated the effects of the compositional asymmetry on lipid rotational dynamics (by way of a rotational autocorrelation function) where we find an effect on the same order as the tilt and order parameter (∼10%, see Table 2). On the other hand, we find only a slight effect of asymmetry on lipid diffusion (∼5%, Table 2 and Figure S6).

L_o/L_d Domain-Height Mismatch. Our simulations comparing compositionally symmetric, phase separated bilayers where we varied the length of the saturated lipid reveal how a mismatch in L_o/L_d domain height, within a leaflet, impacts the communication between leaflets. Figure 4 presents the lateral distributions from these simulations (the di-4:0 data are the same as presented in Figure 2). Whereas in the short-chain, symmetric [di-4:2, di-4:0, Chol]/[di-4:2, di-4:0, Chol] bilayer the domains are in register, domains in the symmetric bilayers containing longer-chained saturated lipids ([di-4:2, di-5:0, Chol]/[di-4:2, di-5:0, Chol] and [di-4:2, di-6:0, Chol]/[di-4:2, di-6:0, Chol]) adopt an antiregistered, phase asymmetric configuration. Figure 5 shows representative snapshots and highlights the near-perfect antiregistration of domains in the two leaflets. Also apparent

dx.doi.org/10.1021/ja106626r |J. Am. Chem. Soc. 2011, 133, 6563–6577

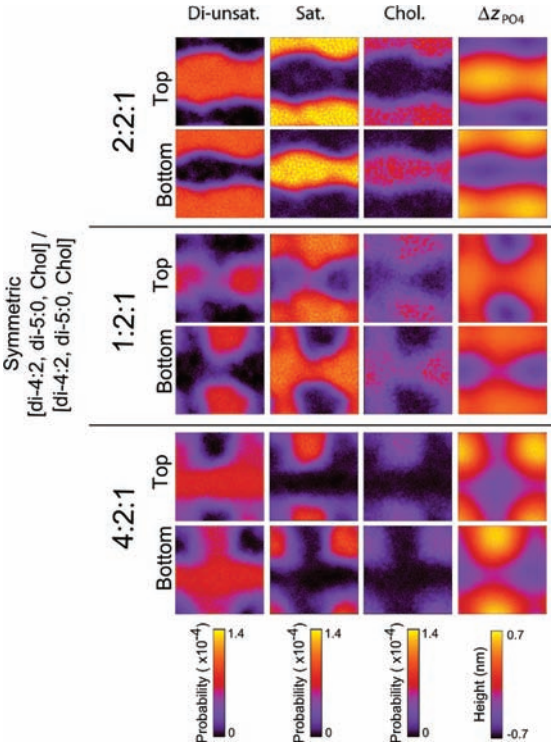

Figure 6. The effect of molar ratios on compositionally symmetric [di-4:2, di-5:0, Chol]/[di-4:2, di-5:0, Chol] bilayers. The near perfectly antiregistered 2:2:1 bilayer is the same as presented above, while the bilayers with different ratios of L_o:L_d show different extents of registration.

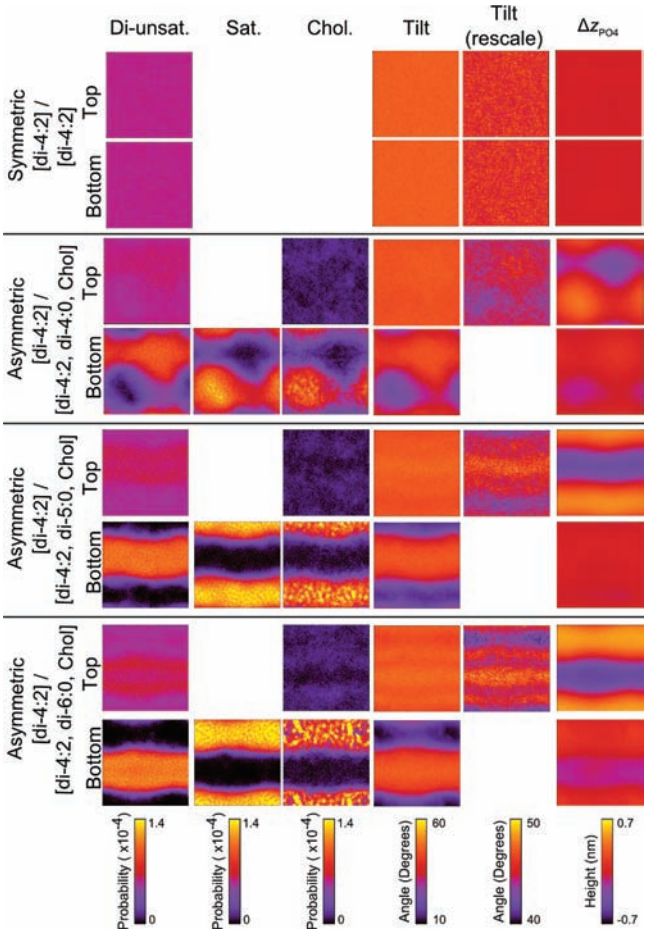

Figure 7. The coupled effect of asymmetry and chain length on per-leaflet component distributions (diunsaturated, saturated, and cholesterol), lipid tilt, and surface curvature for the [di-4:2]/[di-4:2], [di-4:2]/[di-4:2, di-4:0, Chol], [di-4:2]/[di-4:2, di-5:0, Chol], and [di-4:2]/[di-4:2, di-6:0, Chol] bilayers.

in Figure 4, increasing the chain-length of the saturated lipid changes the domain morphology. First, there is a change in domain shape from rounder to straighter stripes, which reduces the contact area between the two domains. Second, the intensity of the profiles in the domains increases as the constituents become more fully segregated into their respective domains. Both of these observations, reduced domain perimeter and increased cohesiveness, indicate that the line tension at the L_o/L_d phase boundary is increased by the height-mismatch.

Table 2 presents the results for tilt, rotational autocorrelation, and diffusion for these L_o domains containing the longer-chained saturated lipids. Increasing the length from 4:0 to 5:0 increases the saturated lipid tilt by ~10%, though further increasing to 6:0 has little effect. Increased chain-length also decreases the rotational freedom and diffusion of the saturated lipids. Importantly, the magnitudes of each of these averaged lipid properties is still within a range characteristic of the L_o phase, rather than the solid phase.[62] In these symmetric, longer-chained antiregistered bilayers, the di-4:2 lipid is perhaps slightly more ordered than in the symmetric bilayer containing the shorter-chained di-4:0. As Table 2 shows, there is an increased effect on the lipid tilt (an additional decrease of ~0.5° and ~1.4°), though there is no clear effect on lateral diffusion or rotational dynamics.

Antiregistration of domains across the bilayer is expected to reduce the energetic penalty associated with hydrophobic exposure of the L_o domain lipids in the case of domain-height mismatch, as has been predicted by theory.[39] However, the near-perfect antiregistration observed in Figures 4 and 5 for the symmetric, long-chained bilayers is only possible because the lateral areas of the two domains are roughly equal at the 2:2:1 mol ratio. It is tantalizing to try to understand the balance of forces that appears to favor an L_o/L_d interface at the bilayer center over the penalty associated with domain-height mismatch in these longer-chain bilayers. To do so, we simulated an additional set of compositionally symmetric [di-4:2, di-5:0, Chol]/[di-4:2, di-5:0, Chol] bilayers where we altered the lipid molar ratios (and hence domain area ratios) in order to see what happens if we force regions of registration. The top two rows of Figure 6 present the results from the 2:2:1 mixture showing the near perfect antiregistered configuration (same data as in Figure 4). The middle two rows present a 1:2:1 mixture which we built expecting twice as much L_o/L_o (registration) as L_d/L_o (antiregistration) overlay between the leaflets. Figure 6 shows that, unlike the 2:2:1 mixture, there are small regions of L_o/L_o overlap, most clearly observed in the corners of the saturated lipid density panels. It appears, however, that despite the proportional doubling of the L_o domain components, L_o/L_o overlap is largely avoided. Instead of overlaying, the data suggest that the domains become more diffuse via changes in the lateral packing within each leaflet (compare intensities in the 2:2:1 and 1:2:1 mixtures in Figure 6). Additionally, and again in contrast to the 2:2:1 bilayer, there are regions with increased mixing, even regions that appear entirely mixed (seen as hazy purple in the figure, most notably at the domain peripheries).

dx.doi.org/10.1021/ja106626r |J. Am. Chem. Soc. 2011, 133, 6563–6577

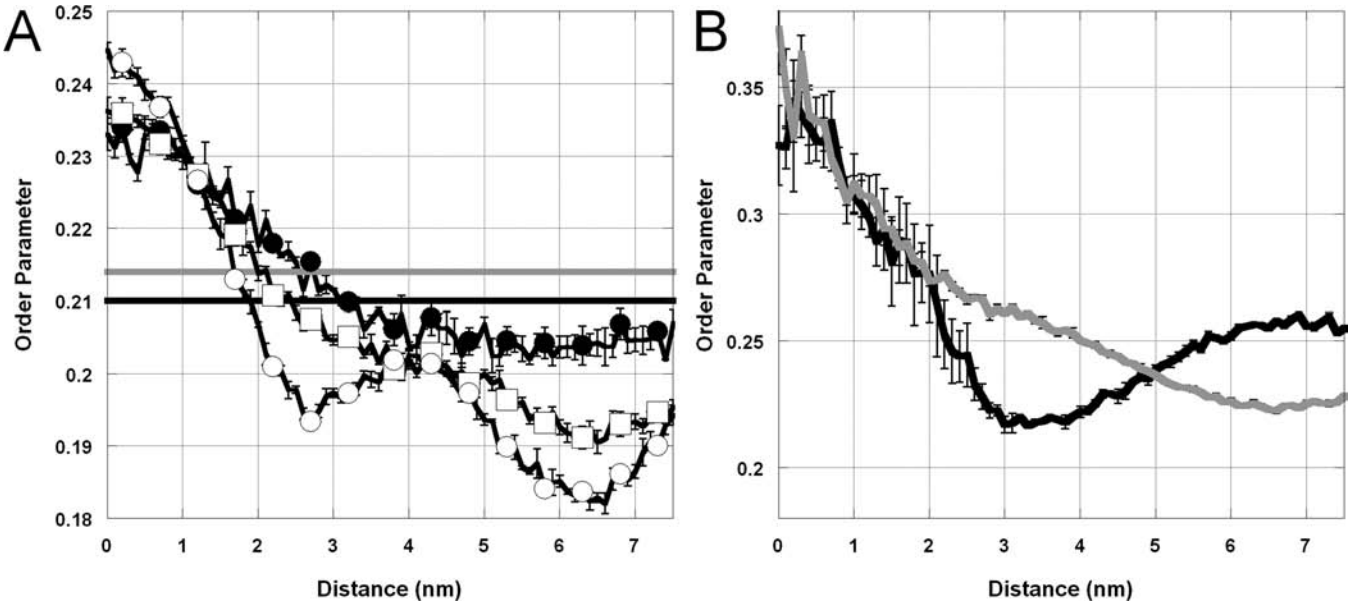

Figure 8. A) The di-4:2 order parameter in the top leaflets of [di-4:2]/[di-4:2, di-4:0, Chol] (black circle), [di-4:2]/[di-4:2, di-5:0, Chol] (open squares), and [di-4:2]/[di-4:2, di-6:0, Chol] (open circles) as well as the control simulations [di-4:2]/[di-4:2] (black) and [di-4:2, 10 Chol]/[di-4:2, 10 Chol] (gray). B) The di-4:2 order parameter in the top leaflet of [di-4:2, di-5:0, Chol]/[di-4:2, di-5:0, Chol] (black) and bottom leaflet of [di-4:2]/[di-4:2, di-5:0, Chol] (gray).

The lowest two rows of Figure 6 present the results of a 4:2:1 mixture, where we had intended to force a substantial degree of L_d/L_d overlap, which in this case is indeed what we observed. The contrast in the extent of L_d/L_d overlap here, as compared to the lack of L_o/L_o overlap at the 1:2:1 ratio, raises an intriguing question regarding the relative energetic penalties of domain-height mismatch and lipid-mixing, namely how the relative compressibility moduli of the two domain-types (greater in the L_o case) dictate the likelihood of domain registration.

Increasing the saturated lipid chain-length also has an effect on the compositionally asymmetric bilayers. Figure 7 presents results for three simulations of asymmetric bilayers containing a top leaflet of di-4:2 and bottom leaflets containing 2:2:1 ternary mixtures where we have varied the chain-length of the saturated lipid. As in Figure 4, increased chain-length causes the domains in the bottom leaflet to become denser and change from rounded to striped. As in the asymmetric bilayer containing di-4:0, there is an interleaflet ordering effect, observed as a reduction in tilt in the region opposite the L_o domains. However, there is also a disordering effect: increased chain-length increases the population of di-4:2 lipids in the top leaflet with higher tilts (hotter colors), in particular in regions of the top leaflet that are directly opposite the L_d phase. This may be why there is a slight increase in average tilt values compared to the di-4:0 case (Table 2). There was weak evidence of this type of disordering across from L_d domains in the asymmetric [di-4:2]/[di-4:2, di-4:0, Chol] bilayer as well, seen as a decrease in order parameter (Figure 3B, distances >3 nm), though in that case the effect was small compared to the ordering opposite the L_o domain. This result is reconfigured into a one-dimensional representation in Figure S7.

Figure 8 more fully describes this interleaflet ordering effect in the bilayers containing long-chain lipids, with comparison to the short-chain case. Figure 8A gives the average order parameter of di-4:2 lipids in the top leaflets of the asymmetric bilayers as a function of distance from the position within the leaflet that is directly opposite the center of the L_o domain in the opposing, phase separated leaflet. As was the case in the [di-4:2]/[di-4:2, di-4:0, Chol] bilayer, and consistent with the tilt data, the ordering effect is greatest in the region directly opposing the center of the L_o domain. The maximal degree of ordering is increased with chain-length, reaching an ~15% increase over control levels, but the ordering falls off much more quickly, perhaps a consequence of the more highly segregated/denser L_o domains (cf. Figure 7). Again consistent with the tilt data, in the regions of the top leaflet directly opposite an L_d domain there is a decrease in order relative to control of as much as almost 15%, nearly the exact magnitude of the ordering effect seen opposite the L_o domain.

Figure 8B confirms that, as expected, in the long-chain, compositionally symmetric antiregistered bilayers, there is both an inter- and intraleaflet ordering effect (refer back to Figure 4 for corresponding density profiles). The figure presents the order parameter data for the [di-4:2, di-5:0, Chol]/[di-4:2, di-5:0, Chol] bilayer, though similar trends are found in the di-6:0 containing bilayer as well (Figure S8). In this case, the appropriate control for distinguishing the inter- from intraleaflet effects is the order parameter for the di-4:2 lipid in the bottom leaflet of the asymmetric [di-4:2]/[di-4:2, di-5:0, Chol] bilayer, in which case there is an intraleaflet effect on the lipid order (due to the ordering imposed by the L_o domain within the bottom leaflet), but no interleaflet effect (the opposing leaflet contains only di-4:2). In the plot, the L_o domain from both simulations is centered at 0 nm. In the control, the di-4:2 is highly ordered (maximum of ~0.35) in the L_o domain, which is also the case in the symmetric, antiregistered bilayer. Outside of the L_o domain, the di-4:2 order parameter drops off sharply, though in quite different ways in the two different cases. The profile is as expected in the control case, where the intraleaflet effect is gradually, and fully screened as the lipid moves further from the domain, reaching a minimum of ~0.22 which is roughly the value of di-4:2 in the single-component L_d bilayer (Figure 8A). In the antiregistered,

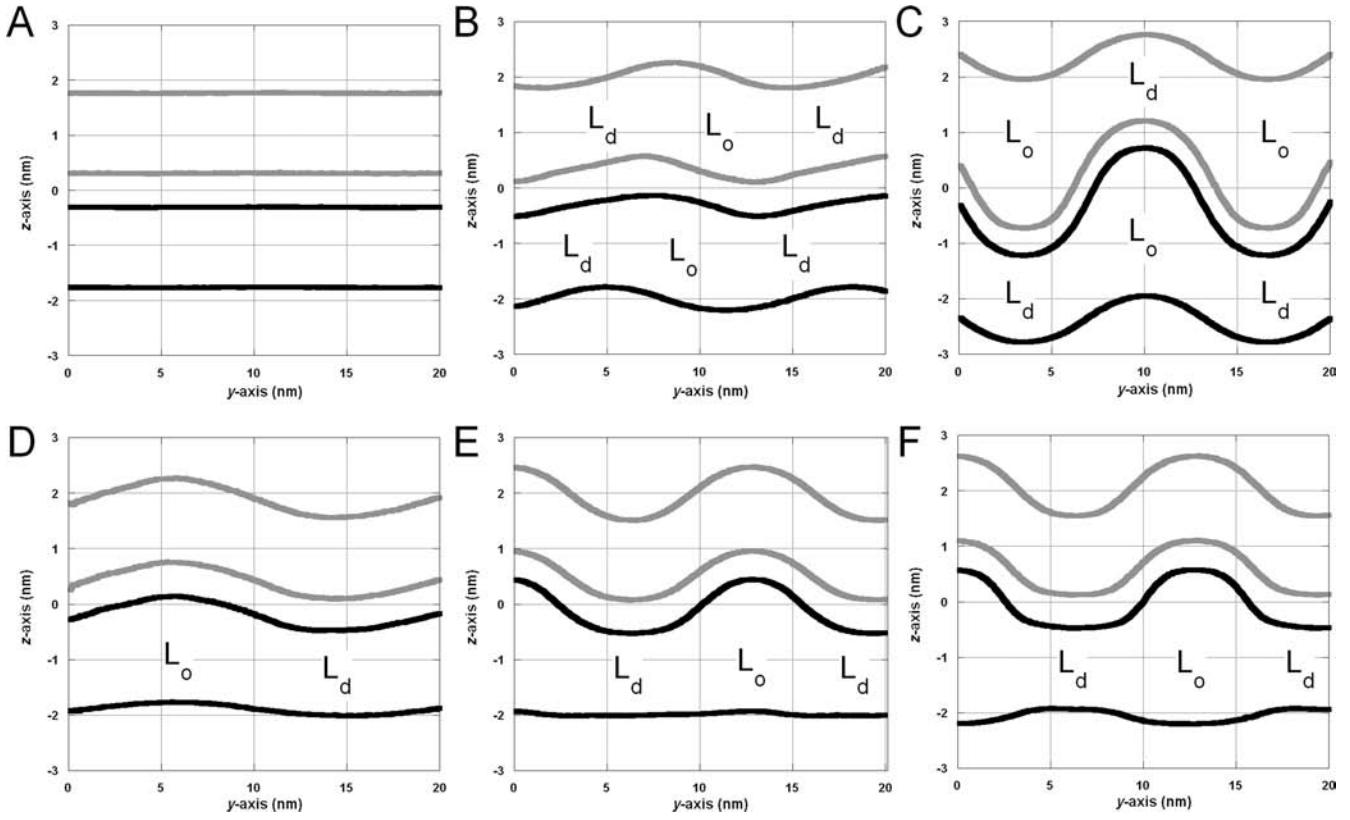

Figure 9. The height of the surfaces composed either of the top leaflet phosphate or terminal tail groups (gray) and bottom leaflet phosphate or terminal tail groups (black) for both saturated and diunsaturated lipids. (A) [di-4:2]/[di-4:2], (B) [di-4:2, di-4:0, Chol]/[di-4:2, di-4:0, Chol], (C) [di-4:2, di-6:0, Chol]/[di-4:2, di-6:0, Chol], (D) [di-4:2]/[di-4:2, di-4:0, Chol], (E) [di-4:2]/[di-4:2, di-5:0, Chol], (F) [di-4:2]/[di-4:2, di-6:0, Chol]. Note that the *x*- and *y*-axes have a different relative scale in order to emphasize the curvature. Corresponding data for the other simulations are available as Figure S9.

symmetric bilayer, outside the L_o domain the di-4:2 lipid experiences both this diminishing intraleaflet effect as well as the interleaflet effect due to the opposing, antiregistered L_o domain. The profile drops off much more sharply in this case (to a minimum of again ~0.22 at a distance of ~3.5 nm). This particular feature of the order parameter profile is quite surprising but in the next section may be explained by a correlation between lipid order and local bilayer curvature. Finally, far from the L_o domain, where the intraleaflet effect is no longer felt, the interleaflet effect takes over (present here because of the antiregistered configuration), and the di-4:2 order increases to ~0.26. This is very similar to the extent of ordering that we see in the L_d domain opposite an L_o domain in the single-component leaflet of the asymmetric bilayer (Figure 8A).

Induction of Curvature in Asymmetric Bilayers. The last columns of Figures 2, 4, 6, and 7 present what are perhaps our most novel findings, namely the effects of compositional asymmetry and domain-height mismatch on the curvature of individual leaflet surfaces. To measure curvature, for each leaflet we defined the average phosphate height and then calculated a Δz_{PO4} for each lipid's phosphate bead relative to that average, binning the data in the *xy*-plane. Positive values (hot colors) indicate outward projections from the bilayer center (for either leaflet). In the [di-4:2]/[di-4:2] bilayer, both leaflets are uniformly flat, as indicated by the value of zero throughout the surface. It is important to note that flatness does not reflect an absence of the normal dynamic motions in the *z*-axis (undulations)[78] but is rather a consequence of the time average of those undulations being zero. The magnitude of these fluctuations is described by the root-mean-square deviation for the distance from each phosphate group to an average flat surface, which for each leaflet of the [di-4:2]/[di-4:2] bilayer is ~0.3 nm. That is, at any individual time point there are thermal fluctuations of this magnitude away from a flat surface, however in the [di-4:2]/[di-4:2] case there is no time-averaged surface curvature.

Quite in contrast, all of the simulated bilayers containing at least one phase separated leaflet are curved. Figure 9 recasts the two-dimensional Δz_{PO4} data presented earlier in one-dimension, presenting a clarifying view of how curvature is communicated from one leaflet to the other in these complex mixtures. As already noted, there is no time-averaged curvature in the single component [di-4:2]/[di-4:2] bilayer (Figure 9A). The calculation of these surfaces is based upon the center of each coarse-grained bead, so that despite the apparent gap at the center of the bilayer (between the terminal methyl surfaces from each leaflet) there is in fact no empty space. Figure 9B shows that in the symmetric [di-4:2, di-4:0, Chol]/[di-4:2, di-4:0, Chol] bilayer, the L_o domains extend further outward than the L_d domains in both leaflets. That this is the case suggests a degree of domain-height mismatch even in the case of L_o domains composed of the shorter-chain saturated lipids. Figure 9C shows that in the compositionally symmetric [di-4:2, di-6:0, Chol]/[di-4:2, di-6:0, Chol] bilayer, increasing the domain-height mismatch increases surface curvature. The curvature profile in the compositionally symmetric di-5:0 bilayer is similar (Figures S9 and S10). In both of the antiregistered bilayers, the L_o domains curves

inward and appear to push out the L_d domains (opposite of what is seen in the registered [di-4:2, di-4:0, Chol]/[di-4:2, di-4:0, Chol] bilayer). In all of the phase separated, symmetric bilayers the curvature is apparent at both the headgroup and terminal methyl surfaces. In the di-5:0 and di-6:0 cases, the headgroup surface is quite curved, but the methyl surfaces are significantly more so, allowing for a striking 'interlocking' of these antiregistered domains at the bilayer center.

This 'interlocking' effect reflects a drive to avoid domain height-mismatch (and resulting curvature strain). Registration of di-5:0 or di-6:0 L_o domains would lead to much sharper transitions between height-mismatched domains and is thus not seen (Figures 4 and 5). We imagine two mechanisms that could resolve height-mismatch: domain antiregistration or domain registration with a large degree of mixing at the domain boundaries. We observe the former, suggesting that the mixing penalty is larger than the penalty due to antiregistration (which we will discuss below). However, in the 1:2:1 and 4:2:1 bilayers (Figure 6), the domains are unable to "perfectly" antiregister, and thus there is a height mismatch between neighboring regions of phase symmetry (either L_o/L_o or L_d/L_d) and phase asymmetry (L_o/L_d). In these cases we do observe an increase in mixing at the domain boundaries. Though mixing is energetically unfavorable, it is apparent that in this case, the penalty is less than the penalty due to extreme curvature.

The corresponding curvature effects in the asymmetric bilayers, shown in Figure 9D-F, are quite remarkable. First, the surfaces of the top, single component leaflets are not flat (compare with the [di-4:2]/[di-4:2] in Figure 9A); rather they project outward in the region opposing the L_o domain (that is, the L_o domain in the bottom leaflet induces a local positive curvature in the top leaflet), and it projects inward in the region opposite the L_d domain (the L_d domain in the bottom leaflet induces a local negative curvature in the top leaflet). Second, the bottom leaflets in these asymmetric bilayers are relatively flat compared to the more curved surfaces in the corresponding symmetric bilayers (Figure 9B and 9C). As the saturated lipid chain-length is increased, the L_o/L_d thickness difference manifests at the terminal methyl surfaces. This curvature is matched by the top leaflet, both in the bilayer center and in the headgroups. As the ordered domain gets thicker, the curvature on the top leaflet gets larger. Thus it appears that the bottom, phase separated leaflets resist curvature in their headgroups and that the major impact of domain-height mismatch in the bottom leaflet manifest in the top, single-component leaflet as an induced leaflet curvature.

As described in the Methods section, we have been exceptionally careful in minimizing any potential leaflet−leaflet area mismatch in our simulated bilayers through our approach to system construction. To further ensure that these curvature phenomena are not due to a buckling effect of area mismatch, we have run a control simulation in which we dramatically altered the area of one of the two leaflets (by removing a number of lipids). The result of that control (Figure S11) is well-substantiated evidence that the curvature effects in these simulated bilayers are a real consequence of differences between the L_o and L_d phases, namely their respective thicknesses and resistance to bending in the individual leaflets, and not an artifact of area mismatch.

It is quite illuminating to compare the curvature profiles in Figure 9 to the order parameter data from Figure 8. In doing so, a clear correlation emerges between surface curvature in the top, single component leaflet and the induced interleaflet ordering effect. For each of the three asymmetric bilayers, in regions opposite L_o domains the top leaflet has positive curvature and the

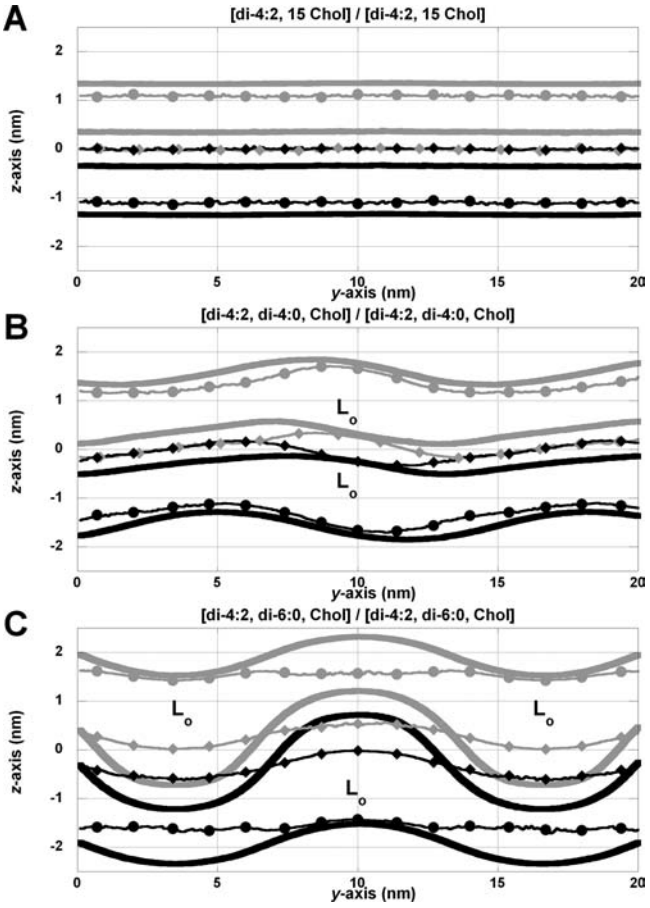

Figure 10. Positions of lipid backbone (solid), terminal methyl (solid), cholesterol hydroxyl (circle), and cholesterol tail (diamonds) for the top (gray) and bottom (black) leaflets of selected simulations. Additional simulations are available as Figure S12.

di-4:2 lipids in that region have an increased order parameter (as well as decreased lipid tilt). Positive curvature suggests increased compression of the chains within the leaflet, offering a likely explanation for their increased order.[79] Conversely, in the regions of the top leaflet that are opposite an L_d domain the leaflet has a negative curvature (decreased chain compression) and the di-4:2 lipids in that region have a decreased order parameter. As was indicated in Figure 8, this effect is increased in the longer chained lipids: larger degrees of surface curvature correlate with larger effects on chain order. The correlation between curvature and order also offers a potential explanation of the data in Figure 8B for the antiregistered bilayers, though this is complicated by the presence of an L_o domain in both leaflets. The di-4:2 order just outside the L_o domain was reduced relative to the control, and as Figure 9C shows the leaflets in those regions have negative curvature. Quite in contrast, in the control case (Figure 9F) those regions are nearly flat.

Cholesterol Position and Interdigitation at the Bilayer Center. The interlocking of domains at the center of the asymmetric bilayers (Figure 9) is somewhat reminiscent of ideas put forth by Sankaram and Thompson in early NMR experiments on the distribution of phospholipids and cholesterol in L_o- and L_d-only bilayers.[59,60] In those studies, the focus was on the leaflet−leaflet interface and the role of interlocking of the constituent molecules between the two leaflets. Our findings

thus far have focused on the interlocking of domains, and here we present a more microscopic view of organization of the constituent molecules. We have probed how the interleaflet interactions described above influence the distribution of molecules in the *z*-dimension (normal to the bilayer). We were specifically interested in whether the lipids and cholesterol molecules interlock (or interdigitate) at the bilayer center.

Figure 10 plots the one-dimensional representations of the bilayers with the average location of the cholesterol headgroups and terminal tail groups now superimposed on the lipid backbone and terminal methyl positions. It is important to remember that the positions of the lines and points in these figures underestimate the extent of the molecular distributions in the *z*-dimension, because they are calculated as the center of the coarse-grained beads, most of which have a radius of ~0.47 nm.[55] Additionally, the data do not reflect the gradient of cholesterol concentration associated with the domains, thus in the L_d domains the average cholesterol positions are taken over many fewer molecules. In each of the simulations, the time-averaged position of the cholesterol hydroxyl is slightly beneath the lipid backbone group. While this is the consensus location of cholesterol, it remains unclear whether it is determined by interaction with the lipid backbone or with water, both of which are thought to occur to some degree.[52,60] Making an unambiguous distinction between these two possibilities is difficult at the CG resolution.

In the [di-4:2]/[di-4:2] bilayer (Figure 10A), the center of the cholesterol tail terminal beads meet at the center, which shows a modest degree of interdigitation of cholesterols. This position for the cholesterols is maintained in the L_d regions of the [di-4:2, di-4:0, Chol]/[di-4:2, di-4:0, Chol] bilayer (Figure 10B). However, in the L_o regions of the same bilayer cholesterol behaves differently. In particular, the cholesterol hydroxyl is closer to the lipid backbone, and the cholesterol tails no longer extend to the bilayer center but instead reach only as far as the lipid terminal methyls. Again, this region of the figure should not be interpreted as indicating empty space at the bilayer center (given that the beads occupy considerable volume beyond their centers). Nevertheless, the data does appear to indicate a slightly diminished molecular density at the L_o/L_o interface that is not present at the L_d/L_d interface. Whether this effect is increased with lipid chain-length is hard to say because of the shift to the antiregistered configuration. However, in the longer-chain data (Figure 10C) the cholesterol tails are even further from the bilayer centers in the L_o regions, a consequence of the strong interactions maintaining the hydroxyl at the depth of the lipid backbones. Quite interestingly, at the L_o/L_d interface at the bilayer center, the cholesterols in the opposing leaflet (in the L_d domain) sink further into the bilayer core, with their tails extending past the bilayer center. This phenomenon also occurs in the asymmetric, long-chained simulations (Figure S12). One possible explanation for this shift in cholesterol position is that these regions may be more permeable to water, though again this is difficult to confirm at the CG resolution.

DISCUSSION

We have organized our study based on two broad mechanisms through which lipid rafts could provide a platform for interleaflet communication. First, in the case of a locally symmetric lipid composition, L_o domains tend to form in the two leaflets in register, resulting in a homogeneous phase across the bilayer (phase symmetry). Conversely, in the case of domain-height mismatch, the domains are antiregistered (phase asymmetry). These antiregistered domains are then subject to the second type of interleaflet organization, which stems from locally asymmetric lipid composition. In this second case, L_o domains in one leaflet can alter the thermodynamic properties of the apposed leaflet. At one extreme, this influence can result in induction of L_o domains despite a lipid composition that would, on its own, favor the L_d phase. This mechanism has been shown in numerous experiments on model systems to depend upon on the specific lipid mixtures and experimental setups. In a less extreme case, where domain formation is not induced, there exists a phase asymmetry, which does not preclude the likelihood that the domains in the one leaflet alter properties of the other without inducing a complete phase change.

We have observed a clear difference in the molecular properties of a di-4:2 leaflet opposite a phase separated leaflet (namely chain tilt and order, rotational dynamics, and curvature). However, whether this justifies recategorizing the phase-state of the leaflet remains unclear. Furthermore, while it is convenient to describe these bilayers as only consisting of two phases (L_d and/or L_o), an alternate, and perhaps more thermodynamically rigorous definition of a region containing phase asymmetry might be as a single, bilayer-spanning 'mixed' phase, as has been postulated based upon recent microscopy experiments.[27] Therefore, these simulations could also be considered the first to describe structural differences between the symmetric and 'mixed' phases.

Experiments on asymmetric bilayers have generally been incapable of interrogating physical properties in a single leaflet, making direct connection with simulations difficult. In the set of fluorescence experiments on asymmetric bilayers two outcomes, or three in the case of Collins et al., have been distinguished by the partitioning of dyes (as determined by visual assignment of fluorescence intensity).[27−30] On the other hand, in simulated bilayer models of L_o/L_d domain separation there is an inherent ambiguity in assigning phase in the same way as the experiments. Most simply put, we do not simulate the partitioning of a dye, though that would in theory be a tractable approach given careful parametrization of the dye chemistry. It is not clear that such a parametrization would be reliable under the coarse-grained simulation strategy, given the subtle chemistry involved, though recent attempts have been promising.[80] Instead, the assignment has typically been made simply by the densities of colocalized constituents (unsaturated lipid in the L_d domain, and saturated lipid and cholesterol in the L_o).

Thus, a vexing issue in analyzing these simulations was whether to assign a phase to the compositionally asymmetric bilayers: is the di-4:2 lipid opposite an L_o domain induced to form the L_o phase, or is it just relatively ordered L_d? In order to answer this question directly from simulations, we would need access to a direct, quantitative relationship between phase and quantifiable lipid properties (e.g., tilt and order) in asymmetric bilayers. Currently, experimental studies on asymmetric bilayers have addressed either phase *or* lipid properties but have not drawn a clear, quantitative relationship between the two. Regarding phase, we have described in detail the experiments which used fluorescent dyes to distinguish between the phases.[27−30] Regarding lipid properties opposite an L_o domain, recent examples include the use of fluorescence anisotropy to describe a decrease in the degree of rotational diffusion (and hence an increase in chain order)[81] and the use of fluorescence correlation

spectroscopy to describe a decrease in the rate of lateral diffusion.[82] However, these studies did not attempt to characterize the phase-state of the altered leaflet.

A probe-free and quantitative experimental method for distinguishing between L_o and L_d domains has recently been established using wide-angle X-ray scattering (WAXS).[83−85] Though this experimental technique is incapable of distinguishing structures in two leaflets, WAXS spectra from simulated bilayers might reasonably be decoupled between the two leaflets. Future simulation efforts might take advantage of that comparison point in establishing the exact phase signature of simulated domains by calculating the WAXS spectra directly from the simulations, though the adequacy of CGMD bilayer simulations to accurately capture X-ray scattering profiles in general has been questioned.[86] Alternate experimental approaches that provide the type of information we have extracted from simulations, such as chain tilt and order (perhaps deuterium NMR experiments on asymmetric bilayers, if only one leaflet could be selectively per-deuterated), would provide a more robust criterion for distinguishing between a relatively ordered L_d phase and the L_o phase in simulations.

Our finding that long-chain saturated lipids (and the resultant domain-height mismatch) leads to domain antiregistration is consistent with a recent theory that suggested that domain registration is dictated by the balance of two tensions.[39] The first is an int*er*-leaflet tension that is predicted to exist between opposing leaflets of different phase and is thus minimized by registration. The second competing tension is an int*ra*-leaflet one, partially caused by height mismatch between neighboring thick (L_o) and thin (L_d) domains—within a given leaflet—that can be ameliorated by antiregistration (see Figures 5 and 9C). Not only does a domain-height mismatch challenge the system with hydrophobic exposure of the chains of the thicker (L_o) domain, it is also likely to incur a curvature stress penalty at the domain boundaries. Our simulations of varied mole ratios (Figure 6) showed that an additional mechanism by which bilayers avoid this apparently costly penalty is through increased mixing of the saturated and unsaturated lipids at the domain boundaries. We see the transition from the registered to antiregistered configurations when the saturated lipid is increased in length from di-4:0 (which models 16-carbon chains) to di-5:0 (20-carbon chains), increasing the L_o/L_d height-mismatch by ∼4 Å. It is quite compelling that this transition occurs near the chain-lengths of most biologically relevant lipids.

An additional consideration regarding the balance of these two tensions is how their relative contributions change with domain size.[39] The magnitude of the interleaflet tension (which is minimized by registration) is dependent upon the domain area, whereas the magnitude of the intraleaflet tension (which is minimized by antiregistration) is dependent upon the domain perimeter. Because a domain's area increases more quickly than its perimeter as it increases in size, all else being equal, we would expect larger domains to favor registration and smaller domains to favor antiregistration. This potentially explains why domain registration is more commonly observed in microscopy experiments than antiregistration, as these experiments are typically done using large domains (tens of micrometers).[27−30,32−34,36] Antiregistration has been observed in simulations of very small (nm) solid domains,[42,43] and has been suggested experimentally,[87,88] including in one notable study of small (<micrometers) solid domains.[38] The presence of antiregistered domains at the length-scale of our simulations is difficult to detect experimentally, and given that biological ordered domains are thought to be as small as tens of nanometers,[4,89] may be a significant observation. It should be noted that we cannot rule out the possibility of finite-size effects in our simulations, though the fact that we see both registered and antiregistered domains indicates that these findings are likely not artifacts of the simulation conditions.

Finally, our findings regarding curvature have bearing on interpretation of experimental observations regarding domain formation and curvature. Experiments in model systems have demonstrated that this type of resistance to curvature is indeed greater in L_o domains than L_d domains, for example as seen in vesicle pipet aspiration.[90−93] It is within this context that our curvature results are particularly compelling. Specifically, in the asymmetric bilayers, we show that the ternary leaflets are flat, but the single-component L_d leaflets are curved. That is, the L_o domains of the bottom leaflets resist curvature to a greater extent than the L_d domains in the top leaflet. This forces the top leaflets to conform to the shape of the bottom leaflet's mismatched acyl chains, resulting in curvature in the top leaflet that likely alters the lipid order. These findings motivate our new hypothesis that induced curvature and associated changes in lipid order is at least one source of interleaflet coupling in asymmetric bilayers. Curvature has been shown to influence membrane protein behavior[64,94−98] and to be an important determinant of intracellular protein trafficking.[64,94,99] Thus, our findings suggest that curvature induced by compositional asymmetry may play an important role in membrane protein localization and function.

■ ASSOCIATED CONTENT

Supporting Information. Supplemental methods and figures. This material is available free of charge via the Internet at http://pubs.acs.org.

■ AUTHOR INFORMATION

Corresponding Author

*Fax: 612-626-6583. E-mail: jnsachs@umn.edu. Corresponding author address: 312 Church St. S.E., 7-126 Hasselmo Hall, Minneapolis, MN 55455.

■ ACKNOWLEDGMENT

The authors thank Dr. Marcus Collins for providing a critical read of the manuscript as well as the three reviewers for their helpful comments and suggestions. Computational resources were provided by the Minnesota Supercomputing Institute (MSI).

■ REFERENCES

(1) Singer, S. J.; Nicolson, G. L. *Science* **1972**, *175*, 720–31.
(2) Engelman, D. M. *Nature* **2005**, *438*, 578–80.
(3) Brown, D. A. *Physiology (Bethesda)* **2006**, *21*, 430–9.
(4) Anderson, R. G.; Jacobson, K. *Science* **2002**, *296*, 1821–5.
(5) Lucero, H. A.; Robbins, P. W. *Arch. Biochem. Biophys.* **2004**, *426*, 208–24.
(6) Simons, K.; Toomre, D. *Nat. Rev. Mol. Cell Biol.* **2000**, *1*, 31–9.
(7) Maxfield, F. R.; Tabas, I. *Nature* **2005**, *438*, 612–21.
(8) Brown, D. A.; London, E. *J. Biol. Chem.* **2000**, *275*, 17221–4.
(9) London, E. *Curr. Opin. Struct. Biol.* **2002**, *12*, 480–6.
(10) Silvius, J. R. *Biochim. Biophys. Acta* **2003**, *1610*, 174–83.

(11) Edidin, M. *Annu. Rev. Biophys. Biomol. Struct.* **2003**, *32*, 257–83.
(12) Veatch, S. L.; Keller, S. L. *Biochim. Biophys. Acta* **2005**, *1746*, 172–85.
(13) Zhao, J.; Wu, J.; Heberle, F. A.; Mills, T. T.; Klawitter, P.; Huang, G.; Costanza, G.; Feigenson, G. W. *Biochim. Biophys. Acta* **2007**, *1768*, 2764–76.
(14) Risselada, H. J.; Marrink, S. J. *Proc. Natl. Acad. Sci. U. S. A.* **2008**, *105*, 17367–72.
(15) Op den Kamp, J. A. *Annu. Rev. Biochem.* **1979**, *48*, 47–71.
(16) van Meer, G.; Voelker, D. R.; Feigenson, G. W. *Nat. Rev. Mol. Cell Biol.* **2008**, *9*, 112–24.
(17) Devaux, P. F.; Morris, R. *Traffic* **2004**, *5*, 241–6.
(18) Bretscher, M. S. *Nat. New Biol.* **1972**, *236*, 11–2.
(19) McIntosh, T. J. *Biophys. J.* **2003**, *85*, 1675–81.
(20) Schroeder, F.; Nemecz, G.; Wood, W. G.; Joiner, C.; Morrot, G.; Ayraut-Jarrier, M.; Devaux, P. F. *Biochim. Biophys. Acta* **1991**, *1066*, 183–92.
(21) Kiessling, V.; Wan, C.; Tamm, L. K. *Biochim. Biophys. Acta* **2009**, *1788*, 64–71.
(22) Ahmed, S. N.; Brown, D. A.; London, E. *Biochemistry* **1997**, *36*, 10944–53.
(23) Wang, T. Y.; Silvius, J. R. *Biophys. J.* **2001**, *81*, 2762–73.
(24) Hunt, G. R.; Tipping, L. R. *Biochim. Biophys. Acta* **1978**, *507*, 242–61.
(25) Schmidt, C. F.; Barenholz, Y.; Huang, C.; Thompson, T. E. *Nature* **1978**, *271*, 775–7.
(26) Sillerud, L. O.; Barnett, R. E. *Biochemistry* **1982**, *21*, 1756–60.
(27) Collins, M. D.; Keller, S. L. *Proc. Natl. Acad. Sci. U. S. A.* **2008**, *105*, 124–8.
(28) Kiessling, V.; Crane, J. M.; Tamm, L. K. *Biophys. J.* **2006**, *91*, 3313–26.
(29) Wan, C.; Kiessling, V.; Tamm, L. K. *Biochemistry* **2008**, *47*, 2190–8.
(30) Garg, S.; Ruhe, J.; Ludtke, K.; Jordan, R.; Naumann, C. A. *Biophys. J.* **2007**, *92*, 1263–70.
(31) Daleke, D. L. *J. Lipid Res.* **2003**, *44*, 233–42.
(32) Samsonov, A. V.; Mihalyov, I.; Cohen, F. S. *Biophys. J.* **2001**, *81*, 1486–500.
(33) Korlach, J.; Schwille, P.; Webb, W. W.; Feigenson, G. W. *Proc. Natl. Acad. Sci. U. S. A.* **1999**, *96*, 8461–6.
(34) Dietrich, C.; Bagatolli, L. A.; Volovyk, Z. N.; Thompson, N. L.; Levi, M.; Jacobson, K.; Gratton, E. *Biophys. J.* **2001**, *80*, 1417–28.
(35) Stottrup, B. L.; Veatch, S. L.; Keller, S. L. *Biophys. J.* **2004**, *86*, 2942–50.
(36) Crane, J. M.; Kiessling, V.; Tamm, L. K. *Langmuir* **2005**, *21*, 1377–88.
(37) Rinia, H. A.; Snel, M. M.; van der Eerden, J. P.; de Kruijff, B. *FEBS Lett.* **2001**, *501*, 92–6.
(38) Almeida, P. F.; Vaz, W. L.; Thompson, T. E. *Biochemistry* **1992**, *31*, 7198–210.
(39) May, S. *Soft Matter* **2009**, *5*, 3148–3156.
(40) Wagner, A. J.; Loew, S.; May, S. *Biophys. J.* **2007**, *93*, 4268–77.
(41) Allender, D. W.; Schick, M. *Biophys. J.* **2006**, *91*, 2928–35.
(42) Khanna, K.; Chang, T. T.; Kindt, J. T. *J. Chem. Phys.* **2006**, *124*, 036102.
(43) Stevens, M. J. *J. Am. Chem. Soc.* **2005**, *127*, 15330–1.
(44) Collins, M. D. *Biophys. J.* **2008**, *94*, L32–4.
(45) Gurtovenko, A. A.; Vattulainen, I. *J. Am. Chem. Soc.* **2005**, *127*, 17570–1.
(46) Lee, S. J.; Song, Y.; Baker, N. A. *Biophys. J.* **2008**, *94*, 3565–76.
(47) Sachs, J. N.; Crozier, P. S.; Woolf, T. B. *J. Chem. Phys.* **2004**, *121*, 10847–51.
(48) Denning, E. J.; Crozier, P. S.; Sachs, J. N.; Woolf, T. B. *Mol. Membr. Biol.* **2009**, *26*, 397–421.
(49) Cascales, J. J. L.; Otero, T. F.; Smith, B. D.; Gonzalez, C.; Marquez, M. *J. Phys. Chem. B* **2006**, *110*, 2358–2363.
(50) Bhide, S. Y.; Zhang, Z.; Berkowitz, M. L. *Biophys. J.* **2007**, *92*, 1284–95.
(51) Vacha, R.; Berkowitz, M. L.; Jungwirth, P. *Biophys. J.* **2009**, *96*, 4493–501.
(52) Kucerka, N.; Perlmutter, J. D.; Pan, J.; Tristram-Nagle, S.; Katsaras, J.; Sachs, J. N. *Biophys. J.* **2008**, *95*, 2792–805.
(53) Gurtovenko, A. A.; Vattulainen, I. *J. Am. Chem. Soc.* **2007**, *129*, 5358–9.
(54) Gurtovenko, A. A.; Vattulainen, I. *J. Phys. Chem. B* **2008**, *112*, 4629–34.
(55) Marrink, S. J.; Risselada, H. J.; Yefimov, S.; Tieleman, D. P.; de Vries, A. H. *J. Phys. Chem. B* **2007**, *111*, 7812–24.
(56) Esteban-Martin, S.; Risselada, H. J.; Salgado, J.; Marrink, S. J. *J. Am. Chem. Soc.* **2009**, *131*, 15194–15202.
(57) Bennum, S. V.; Longo, M. L.; Faller, R. *Langmuir* **2007**, *23*, 12465–12468.
(58) Xing, C.; Faller, R. *J. Phys. Chem. B* **2008**, *112*, 7086–94.
(59) Sankaram, M. B.; Thompson, T. E. *Biochemistry* **1990**, *29*, 10676–84.
(60) Sankaram, M. B.; Thompson, T. E. *Proc. Natl. Acad. Sci. U. S. A.* **1991**, *88*, 8686–90.
(61) Perlmutter, J. D.; Sachs, J. N. *J. Am. Chem. Soc.* **2009**, *131*, 16362–3.
(62) Marrink, S. J.; Risselada, J.; Mark, A. E. *Chem. Phys. Lipids* **2005**, *135*, 223–44.
(63) Sheetz, M. P.; Singer, S. J. *Proc. Natl. Acad. Sci. U. S. A.* **1974**, *71*, 4457–61.
(64) Zimmerberg, J.; Kozlov, M. M. *Nat. Rev. Mol. Cell Biol.* **2006**, *7*, 9–19.
(65) Cheng, H. T.; Megha; London, E. *J. Biol. Chem.* **2009**, *284*, 6079–92.
(66) Pautot, S.; Frisken, B. J.; Weitz, D. A. *Proc. Natl. Acad. Sci. U. S. A.* **2003**, *100*, 10718–21.
(67) Hess, B.; Kutzer, C.; Van Der Spoel, D.; Lindahl, E. *J. Chem. Theory Comput.* **2008**, *4*, 435–447.
(68) Humphrey, W.; Dalke, A.; Schulten, K. *J. Mol. Graph.* **1996**, *14*, 33–38.
(69) Marrink, S. J.; de Vries, A. H.; Harroun, T. A.; Katsaras, J.; Wassall, S. R. *J. Am. Chem. Soc.* **2008**, *130*, 10–1.
(70) Bennett, W. F.; MacCallum, J. L.; Hinner, M. J.; Marrink, S. J.; Tieleman, D. P. *J. Am. Chem. Soc.* **2009**, *131*, 12714–20.
(71) Siwko, M. E.; Marrink, S. J.; de Vries, A. H.; Kozubek, A.; Schoot Uiterkamp, A. J.; Mark, A. E. *Biochim. Biophys. Acta* **2007**, *1768*, 198–206.
(72) Klauda, J. B.; Roberts, M. F.; Redfield, A. G.; Brooks, B. R.; Pastor, R. W. *Biophys. J.* **2008**, *94*, 3074–83.
(73) McIntosh, T. J. *Biochim. Biophys. Acta* **1978**, *513*, 43–58.
(74) Hung, W. C.; Lee, M. T.; Chen, F. Y.; Huang, H. W. *Biophys. J.* **2007**, *92*, 3960–7.
(75) Levine, Y. K.; Wilkins, M. H. *Nat. New Biol.* **1971**, *230*, 69–72.
(76) Pan, J.; Tristram-Nagle, S.; Nagle, J. F. *Phys. Rev. E: Stat., Nonlinear, Soft Matter Phys.* **2009**, *80*, 021931.
(77) Pandit, S. A.; Vasudevan, S.; Chiu, S. W.; Mashl, R. J.; Jakobsson, E.; Scott, H. L. *Biophys. J.* **2004**, *87*, 1092–100.
(78) Lindahl, E.; Edholm, O. *Biophys. J.* **2000**, *79*, 426–33.
(79) Thurmond, R. L.; Lindblom, G.; Brown, M. F. *Biochemistry* **1993**, *32*, 5394–410.
(80) Hinner, M. J.; Marrink, S. J.; de Vries, A. H. *J. Phys. Chem. B* **2009**, *113*, 15807–19.
(81) Megha; Bakht, O.; London, E. *J. Biol. Chem.* **2006**, *281*, 21903–13.
(82) Chiantia, S.; Schwille, P.; Klymchenko, A. S.; London, E. *Biophys. J.* **2011**, *100*, L1–3.
(83) Mills, T. T.; Toombes, G. E.; Tristram-Nagle, S.; Smilgies, D. M.; Feigenson, G. W.; Nagle, J. F. *Biophys. J.* **2008**, *95*, 669–81.
(84) Mills, T. T.; Tristram-Nagle, S.; Heberle, F. A.; Morales, N. F.; Zhao, J.; Wu, J.; Toombes, G. E.; Nagle, J. F.; Feigenson, G. W. *Biophys. J.* **2008**, *95*, 682–90.
(85) Mills, T. T.; Huang, J.; Feigenson, G. W.; Nagle, J. F. *Gen. Physiol. Biophys.* **2009**, *28*, 126–39.

(86) Perlmutter, J. D.; Sachs, J. N. *Biochim. Biophys. Acta, Biomembr.* **2009**, *1788*, 2284–2290.
(87) Zhang, J.; Jing, B.; Tokutake, N.; Regen, S. L. *J. Am. Chem. Soc.* **2004**, *126*, 10856–7.
(88) Zhang, J.; Jing, B.; Tokutake, N.; Regen, S. L. *Biochemistry* **2005**, *44*, 3598–603.
(89) Hancock, J. F. *Nat. Rev. Mol. Cell Biol.* **2006**, *7*, 456–62.
(90) Roux, A.; Cuvelier, D.; Nassoy, P.; Prost, J.; Bassereau, P.; Goud, B. *EMBO J.* **2005**, *24*, 1537–45.
(91) Baumgart, T.; Das, S.; Webb, W. W.; Jenkins, J. T. *Biophys. J.* **2005**, *89*, 1067–80.
(92) Heinrich, M.; Tian, A.; Esposito, C.; Baumgart, T. *Proc. Natl. Acad. Sci. U. S. A.* **2010**, *107*, 7208–13.
(93) Parthasarathy, R.; Groves, J. T. *Soft Matter* **2007**, *3*, 24–33.
(94) McMahon, H. T.; Gallop, J. L. *Nature* **2005**, *438*, 590–6.
(95) Tian, A.; Baumgart, T. *Biophys. J.* **2009**, *96*, 2676–88.
(96) Huang, K. C.; Ramamurthi, K. S. *Mol. Microbiol.* **2010**, *76*, 822–832.
(97) Brown, M. F. *Chem Phys. Lipids* **1994**, *73*, 159–80.
(98) Perlmutter, J. D.; Braun, A. R.; Sachs, J. N. *J. Biol. Chem.* **2009**, *284*, 7177–89.
(99) Mukherjee, S.; Maxfield, F. R. *Traffic* **2000**, *1*, 203–11.